Journal of The Electrochemical Society, **152** (1) A73-A79 (2005)
0013-4651/2004/152(1)/A73/7/$7.00 © The Electrochemical Society, Inc.

Investigations of the Exothermic Reactions of Natural Graphite Anode for Li-Ion Batteries during Thermal Runaway

Hui Yang,[a,*] Hyunjoo Bang,[a,*] Khalil Amine,[b,] and Jai Prakash[a,**,z]**

[a]*Center for Electrochemical Science and Engineering, Department of Chemical and Environmental Engineering, Illinois Institute of Technology, Chicago, Illinois, 60616, USA*
[b]*Argonne National Laboratory, Chemical Technology Division, Argonne, Illinois, 60439, USA*

Advances in the comparative study of the thermal behavior of graphite during the thermal runaway process are reviewed. The differential scanning calorimeter was used to evaluate the thermal runaway behavior of natural graphite (Mag-10) electrode material with different amounts of intercalated lithium ions. The effect of the polyvinylidene fluoride binder on the thermal behavior of a fully lithiated sample was also investigated. This is the first time it has been noted that graphite loses its structure with more than 0.7 intercalated lithium when electrolyte is present at high temperature by detecting the existence of (002) graphite X-ray diffraction peak.
 [DOI: 10.1149/1.1836126]

Manuscript submitted April 12, 2004; revised manuscript received June 18, 2004. Available electronically November 29, 2004.

Lithium-ion rechargeable batteries possess high energy density and excellent power compared to other commercialized battery systems, which give them a significant market as power sources for portable electronics such as cellular phones and laptop computers. However, their applications to electric vehicles (EVs) and hybrid vehicles (HVs) have been limited because these applications need better thermal stability to reduce the safety risks.[1-4] Although many studies have been carried out to improve the safety of Li-ion batteries (such as the development of flame retardant additives,[5] thermally stable cathodes,[6-8] and thermally stable electrolytes[9,10]), there are still some safety concerns associated with the use of Li-ion batteries in EVs and HVs. Safety issues generally occur if the cell exceeds the critical temperature above which the increase of the cell temperature is irreversible (thermal runaway) due to the heat produced by the anode, cathode, electrolyte, and their interactions above the critical temperature.

Differential scanning calorimeter (DSC) and accelerating rate calorimeter (ARC) have been used to investigate the thermal stability of salts, electrolytes, cathodes, anodes, conductive materials, and binder additives.[11-25] The reactions of these individual components have also been correlated with the thermal runaway of full-cells.[11,12] In the DSC studies[11] of $Li_{0.36}Ni_{0.8}Co_{0.15}Al_{0.05}O_2$ and $Li_{0.91}C_6$ (fully charged state), the cathode contributes -815 J and the anode contributes -707 J to the overall exothermic heat generation on the basis of 1 g electrode materials. More than 95% of the heat is generated by the anode from 80 to 180°C; this heat is attributed to the decomposition of solid electrolyte interface (SEI) and the formation of a secondary SEI film. About 74% of the heat is generated by cathode from 180 to 250°C; this heat is produced by the decomposition of the delithiated cathode and the combustion of the electrolyte with liberated O_2. The cathode and anode each contribute half of the heat to the thermal runaway after the temperature exceeds 250°C. Maleki *et al.*[12] also found that the cell thermal runaway was initiated by SEI film breakdown, followed by thermal decomposition/reaction of electrolyte with negative electrode, and finally the thermal decomposition of the cathode and its components. Hence, the mechanisms of thermal runaway reactions for anode materials are useful in understanding the thermal behavior of Li-ion cells; this understanding can lead to the development of new materials with improved safety and stability.

Except for the initiator of the thermal runaway for the Li-ion cells described above, SEI film breakdown and reformation during storage at elevated temperatures (60-80°C) are also responsible for cell gassing.[26,27] The SEI film is a passivating surface film on the graphite particle consisting of Li-alkyl-carbonates, polymeric ethylene carbonate, and lithium fluoride[28,29] and is formed on the surface of graphite particles via either the direct decomposition of the solvents on the basal plane to form a precipitate layer, or the cointercalation of solvated lithium ions and their decomposition beneath the surface in the initial stage of lithium intercalation (exfoliation), mainly in the first and second cycle (passivating surface film).[30,31] Some metastable organic compounds of SEI film decomposition at high temperatures (80-120°C) allow further thermal reactions between the lithiated graphite and the electrolyte. In this study, the DSC behaviors of natural graphite Mag-10 at different states of charge (SOC) are studied and a reaction mechanism for the exothermic reactions during the thermal runaway process is proposed. In addition, thermal stability of the Li-ion anode is greatly improved by selecting a spherical natural graphite (GDR) coated with a thin layer of carbon.

Experimental

Cell fabrication.—The anode laminate is composed of 92 wt % natural graphite (Mag-10) or carbon-coated graphite (CCG, natural graphite GDR coated with 6 wt % carbon), and 8 wt % polyvinylidene fluoride (PVDF) binder. The electrolyte composition is 1.2 M $LiPF_6$ in ethylene carbonate (EC) and ethyl methyl carbonate (EMC) (wt %: 3-7). The coin cells (2032) were fabricated using the anode laminate, electrolyte, a Celgard (3501) surfactant-coated porous polypropylene separator, lithium metal, and a stainless steel case in an argon atmosphere dry box. All chemicals for electrode fabrication were provided by the Argonne National Laboratory.

DSC measurement.—The coin cells were galvanostatically charged and discharged 5 times at 137 $\mu A\ cm^{-2}$ with a BT-2043 Arbin cycler. The high cutoff voltage and low cutoff voltage were set to 1.2 V and 0 V, respectively. The cells were finally discharged to different SOC for DSC measurements.

After opening the cell in the argon-filled dry box carefully, the extra electrolyte was removed from the surface of the electrode and the electrode materials were recovered from the current collector. A stainless steel sealed pan with a gold-plated copper seal (which can withstand 150 atm of pressure before rupturing and has a capacity of 30 μL) was used to collect 3-5 mg samples. The measurements were carried out in a Pyris 1 differential scanning calorimeter from Perkin Elmer Corp. The weight of each sample (pan + sample) was measured before and after the experiment to verify that the system was hermetically sealed. The weight was constant in all cases, indicating that there were no leaks during the experiments. The DSC scans were performed at various heat rates. At least five scans were performed at a scan rate of $10°C\ min^{-1}$ to determine the enthalpy and four runs in the range from 2.5 to $50°C\ min^{-1}$ to calculate the activation energy.

* Electrochemical Society Student Member.
** Electrochemical Society Active Member.
z E-mail: prakash@iit.edu

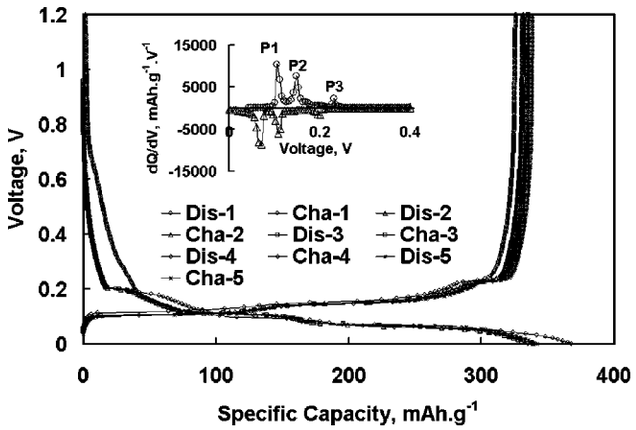

Figure 1. Electrochemical performance of the natural graphite (Mag-10)/Li half-cell cycled at a current density of 137.2 μA cm^{-2}. Inset plot presents the differential capacity *vs.* voltage for the Mag-10/Li half-cell.

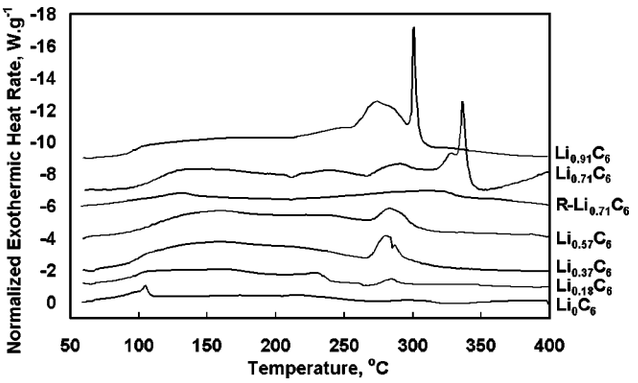

Figure 2. DSC curves of Mag-10 samples with different amounts of intercalated lithium at a scan rate of 10°C min^{-1}. R-$Li_{0.71}C_6$ represents a graphite anode rinsed with DMC and vacuum dried to remove the remaining salt and EC. In Li_xC_6, x represents only the amount of Li inside the graphite matrix; it doesnot include about 0.11 Li in the SEI film compounds on the surface of graphite particles.

The enthalpy of the reaction was determined by integrating a peak of interest from the DSC trace of the power *vs.* time.[32] The activation energy, E_a, and the frequency factor, A, were calculated from the following equation[32,33]

$$\ln\frac{a}{T_m^2} = \ln\frac{AR}{E_a} - \frac{E_a}{RT_m} \quad [1]$$

where a is the heating rate, T_m is the peak temperature, A is the frequency factor, E_a is the activation energy, and R is the gas constant.

X-ray diffraction.—Anode laminates at different states of charge were recovered and placed in sealed small stainless steel cylinders (argon atmosphere inside) and heated to 400°C for 10 min. Then the heated sample powders were collected. Powder X-ray diffraction (XRD) measurements were carried out with a Rigaku Miniflux X-ray diffractometer equipped with Cu K_α radiation. XRD data were collected between 10 and 90° (2θ).

Results and Discussion

The electrochemical cycling performance of Mag-10 graphite in the first five cycles at a current of 68.6 μA cm^{-2} is shown in Fig. 1. The differential capacity of this sample in the fifth cycle is also shown in the inset plot. A plateau observed near 0.65 V in the first discharge process is associated with the decomposition of the electrolyte on the surface of graphite in the formation of the passivating film layer.[34] This plateau disappears in subsequent cycling because the formatted passivating film suppresses further electrolyte decomposition. The irreversible capacity observed in the first cycle for Mag-10 carbon electrode is 42 mAh g^{-1}, suggesting the initial SEI film contains about 0.11 Li per C_6. The other plateaus in low voltage ranges show three different phase transition states (corresponding to three clear peaks in the differential capacity). The clear sharp peaks with large peak separations due to the well-defined phase transition also suggest that this sample has a well-ordered graphite structure.[35]

Figure 2 presents the DSC curves obtained from the lithiated Mag-10 anode samples (every 20% state of charge) at a scan rate of 10°C min^{-1} from 50 to 400°C. This figure shows that only one exothermic peak is detected in the fully deintercalated sample (Li_0C_6). This peak is broadened to a wide peak with more intercalated lithium (Li_xC_6, $x \geqslant 0.18$). A peak starting at 269°C and reaching the maximum at 283°C is detected in the DSC scan of $Li_{0.37}C_6$. A DSC trace of $Li_{0.57}C_6$ is similar to that of $Li_{0.37}C_6$. However, a new sharp peak at about 336°C is detected at the DSC curve for $Li_{0.71}C_6$. This sharp peak shifts to 301°C with more intercalated lithium ($Li_{0.91}C_6$).

The Li_0C_6 sample (0% SOC) contains graphite, SEI film, and the remaining electrolyte (mainly $LiPF_6$ and EC). SEI film comprises stable compounds (LiF, Li_2CO_3, and other inorganic compounds) and metastable components (lithium-alkyl carbonates, lithium semicarbonate). The metastable components are not stable at high temperatures, especially in the presence of Li atoms.[17,28,29,36] The electrolyte employed here does not decompose and produce heat until 250°C.[11,22] In addition, fresh graphite does not react strongly with electrolyte below 190°C.[11,17] Therefore, this peak can be attributed only to the SEI breakdown.[17] The structure and composition of the SEI film is complex and contains several inorganic and organic compounds. All these compounds may participate in the SEI decomposition reaction. However, one most possible reaction mechanism may be

$$(CH_2OCO_2Li)_2 \rightarrow Li_2CO_3 + C_2H_4 + CO_2 + 0.5\ O_2$$

The peak associated with the SEI film decomposition increases with increasing intercalated lithium, as shown in the curves for Li_xC_6 ($x \geqslant 0.18$). There are two possibilities for the peak broadening associated with the SEI breakdown. First, the covered surface that is initially present is exposed due to the melting of the PVDF and fresh SEI film is formed through the reaction between the intercalated Li and electrolyte.[24] Also, the intercalated Li can react with $(CH_2OCO_2Li)_2$ compound as[17]

$$2Li + (CH_2OCO_2Li)_2 \rightarrow 2Li_2CO_3 + C_2H_4$$

Some other inorganic compounds, such as LiF, are also formed at this temperature. $LiPF_6$ salt decomposes at 70°C and produces LiF and a thermally stable gas, PF_5.[37-40] Also, the existence of a trace amount of moisture can cause the following reactions[40]

$$LiPF_6 + H_2O \rightarrow 2HF + LiF + POF_3$$

$$2HF + Li_2CO_3 \rightarrow 2LiF + H_2CO_3$$

It has been shown[20,40,41] that the amount of LiF increases with increasing storage temperature. Lee *et al.*[26] reported that PF_5 was the major species responsible for the destruction of the SEI layer at high temperatures. Because PF_5 is a strong Lewis acid and attacks the electron lone pair or the atom with a large electron density, it is likely to react with the oxygen atom of carbonyl groups (-C = O) and compounds possessing sites of increased electron density. In

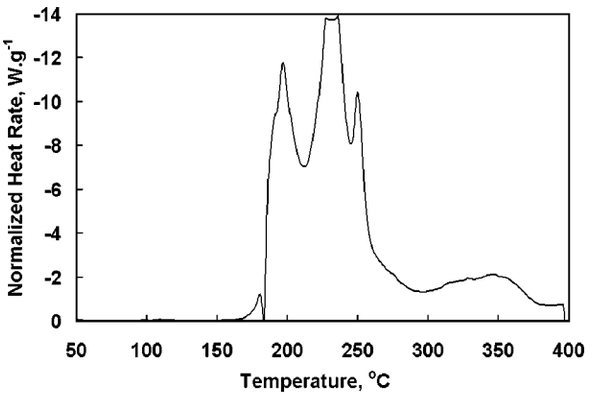

Figure 3. DSC scan of Li metal with electrolyte at a heat rate of 10°C min^{-1}.

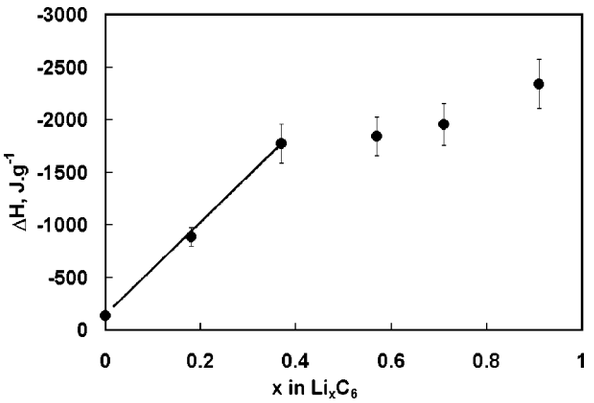

Figure 4. Overall heat generation of anode samples with different amounts of intercalated Li.

addition, the dominant component of the SEI is $(CH_2OCO_2Li)_2$, indicating the C-O functional group. Hence, it is reasonable to propose that PF_5 damages the SEI in a $LiPF_6$ system at 80°C.[26]

In the DSC scan of $Li_{0.18}C_6$, the heat rate after SEI film decomposition does not drop to zero until 240°C, indicating that there are some new reactions following the SEI decomposition. This mild broad peak is enlarged when more lithium ions intercalate, as illustrated in the DSC traces of $Li_{x>0.37}C_6$. This reaction disappears in the rinsed $Li_{0.71}C_6$ sample [shown in curve R-$Li_{0.71}C_6$, which was rinsed with dimethyl carbonate (DMC) and vacuum dried to remove all the salts and EC]. In addition, this peak is absent in the fully deintercalated sample (Li_0C_6). Therefore, this peak may be attributed to the reaction between the intercalated lithium and the electrolyte. Three sharp peaks were detected in the temperature range from 170 to 300°C (Fig. 3) in the DSC scan of Li metal and the electrolyte. Von Sacken *et al.*[14] also reported that the Li metal anode (after a few cycles) reacted with electrolyte more violently than the fresh metal. SEI film compounds contain electronically insulating $(CH_2OCO_2Li)_2$ surface film which avoid further cointercalation of solvent molecules and/or exfoliation of the graphite surface, hence allowing only Li^+ migration.[29,42] The $(CH_2OCO_2Li)_2$ present on the surface film is removed after the SEI film breakdown at elevated temperature. Thus the salts and the electrolyte can permeate the Li_2CO_3 and LiF film to reach the lithiated graphite surface. It has been reported[26,41,43] in literature that the intercalated Li ions move from the inner structure to the edge of graphite particles at high temperatures. Lee *et al.*[26] claimed that lithium in carbon was highly active at high temperatures and high temperatures can accelerate lithium loss from the carbon matrix. They observed the apparent color change of the carbon electrodes from golden (intercalated state) to black (deintercalated state) during storage of cells at 80°C. Andersson and Edstrom[41] showed the amount of lithium changed from LiC_6 (stage 1) to LiC_{12} (stage 2) during storage at 80°C by monitoring the *in situ* XRD measurement. Edstrom *et al.*[43] also noted that 50% of the lithium ions were lost from the graphite after a 12 h storage at 60°C. Hence, a secondary SEI film forms when intercalated lithium reacts with the electrolyte. Most probably only stable compounds, such as Li_2CO_3 and LiF, are formed at that high temperature[44]

$$(CH_2)_2OCO_2 + 2Li \rightarrow C_2H_4 + Li_2CO_3$$

$$PF_5 + 2xLi \rightarrow Li_xPF_{5-x} + xLiF$$

$$POF_3 + 2xLi \rightarrow Li_xPOF_{3-x} + xLiF$$

Several studies[13,17,24,45] have also concluded that intercalated lithium reacted with the electrolyte to form a new stable SEI film after SEI decomposition at the edge planes. This is consistent with what was reported by Edstrom and Herranen[18] who noted that the reaction products on highly oriented pyrolytic graphite (HOPG) were formed predominantly at the edge planes. The formation of secondary SEI film reactions stops when either the new film is too thick or all the intercalated Li has been consumed. Figure 4 shows the overall enthalpy values for the exothermic reactions of Li_xC_6 with different amounts of intercalated lithium. More intercalated lithium results in larger enthalpy values, indicating that the graphite anode has the higher potential to undergo thermal runaway with a higher SOC. Richard and Dahn[17] also noted that the most intercalated Li sample had the highest self-heat rate and required the least time to reach end point in the ARC test. Assuming the formation of Li_2CO_3 is the main reaction in forming secondary SEI film, the enthalpy value is produced by the reaction of intercalated Li and the electrolyte, and should be proportional to the amount of consumed Li in this reaction. Clearly from this figure, the enthalpy is proportional to the lithium content when x is less than 0.37. However, the enthalpy increases slowly for $x > 0.37$, indicating that the formation of secondary SEI film stops after 0.37 Li has been consumed. Dahn *et al.*[16,17] claimed that about 0.3 M of Li were consumed in the exothermic reaction up to 220°C in their ARC studies of several graphite samples. Even in a fully intercalated state, 80% of the heat is produced by the SEI decomposition and the formation of a stable SEI film.

A peak starting at 269°C and reaching maximum at 283°C is detected in the DSC scan of $Li_{x>0.37}C_6$ samples (Fig. 2). The cause of this peak is unknown and needs further investigation. A very sharp peak is detected in the DSC scans of the samples intercalated with more than 0.7 lithium per C_6 ($Li_{0.71}C_6$ and $Li_{0.91}C_6$). Du Pasquier *et al.*[45] and Maleki *et al.*[12,21] attributed this sharp peak to the reaction of the PVDF binder with the lithiated graphite. Yamaki *et al.*[24] suggested that the sharp exothermic peak at 280°C was the direct reaction of the lithiated graphite and electrolyte due to SEI breakdown. However, this peak disappears in the rinsed sample (R-$Li_{0.71}C_6$). We believe that the salts and/or EC are also involved in this reaction. This peak shifts to lower temperature with a large exothermic heat rate when more lithium ions intercalate ($Li_{0.91}C_6$). To understand the involvement of PVDF binder in this reaction, we fabricated a Mag-10 pellet without the PVDF binder.[24] A coin cell fabricated with this pellet was cycled five times and then fully discharged. The composition of this pellet-type electrode after being fully intercalated was $Li_{1.0}C_6$. Two DSC scans were conducted after recovering the fully lithiated golden graphite powders: the DSC scan of the fully intercalated Mag-10 and the DSC scan of the fully intercalated Mag-10 with 12 wt % PVDF as shown in Fig. 5. The sharp peak observed at ~300°C in Fig. 2 still appears in the DSC trace of the $Li_{1.0}C_6$ sample without PVDF in Fig. 5 (at ~270°C). However, this peak shifts to a higher temperature (~290°C) and the

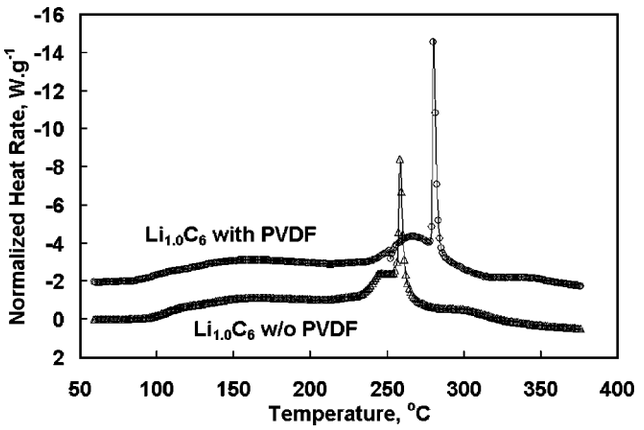

Figure 5. DSC scan of $Li_{1.0}C_6$ with and without PVDF binder.

peak height increases with added PVDF. Based on this result, we conclude that PVDF is not necessary to cause this peak. Du Pasquier *et al.*[45] noted that heat generation with 10 wt % PVDF was 23% higher than the sample with mixed PVDF: hexafluoropropene (HFP). Maleki *et al.*[21] also claimed a significant reduction in total heat generation and a slightly lower peak temperature when PVDF was fully or partially replaced by phenol-formaldehyde (PF).

Figure 6a and b presents the XRD patterns of intercalated Mag-10 samples after heating in a sealed argon atmosphere cylinder at 400°C for 10 min. The characteristic 002 peak of graphite is detected for samples Li_0C_6, $Li_{0.18}C_6$, $Li_{0.37}C_6$, $Li_{0.57}C_6$, and R-$Li_{0.71}C_6$ as shown in Fig. 6a. The sample with more intercalated Li has a slightly broadened full width at half-maximum (fwhm) in 002 peak indicating that the graphite particles are becoming smaller after the formation of the secondary SEI film. The graphite structure can expand up to 10% in a fully intercalated state in the 002 direction.[46] EC and $LiPF_6$ can enter into the graphite sheets at high

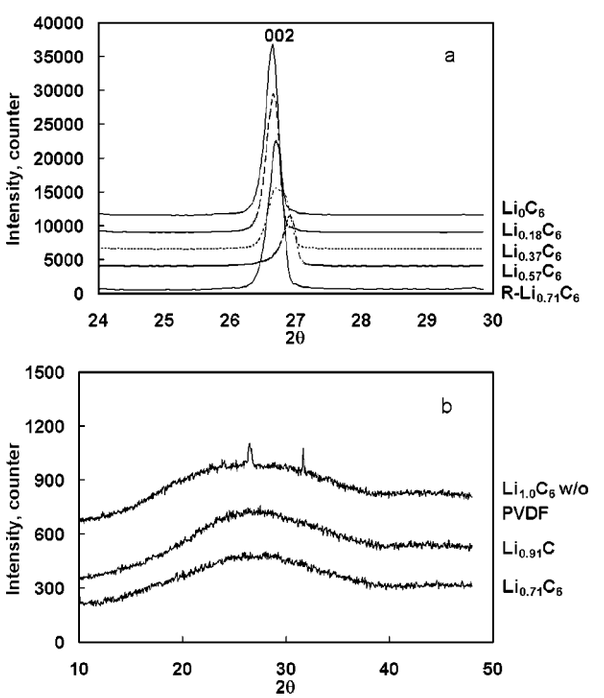

Figure 6. XRD patterns of lithiated graphite samples heated at 400°C for 10 min.

pressure and react with intercalated lithium to form lithium carbonate and ethylene. This process may be similar to the exfoliation in the first cycle of Li intercalation and can bring about significant changes in the surface structure including the breakdown of the graphite powder into fragments. Ghung *et al.*[47] claimed that exfoliation did not appear to destroy the bulk structure completely, but brought about significant changes in the surface structure, such as the exfoliation of the surface layers of graphite, and the fracture of the graphite powder into fragments. Aurbach *et al.*[44] also noted that structural changes occur during exfoliation. It is surprising that $Li_{0.71}C_6$, $Li_{0.91}C_6$, and $Li_{1.0}C_6$ lose their graphite structure at high temperature. Therefore the sharp peak detected for $Li_{0.71}C_6$, $Li_{0.91}C_6$ samples in Fig. 2, and $Li_{1.0}C_6$ sample in Fig. 5 may be attributed to the collapse of the graphite structure. Clearly from Fig. 6a, the R-$Li_{0.71}C_6$ sample maintains the graphite structure even after heating at 400°C. Also, no sharp peak is detected in the DSC trace of this sample (Fig. 2, curve R-$Li_{0.71}C_6$). These observations suggest that $LiPF_6$/EC and/or their decomposition by-products are most likely responsible for the structural collapse. Based on the above discussion, we may explain the increased peak height of the sharp peak for sample $Li_{1.0}C_6$ with added PVDF (Fig. 5) as follows. The released Li from the collapsed graphite particles can react with PVDF at this high temperature and produce more heat. This reaction can be attributed to the dehydrofluorination of PVDF and formation of LiF and hydrogen.[48]

Because SEI film is the initiator of thermal runaway of Li-ion cells, anode with less SEI film formation should have better thermal behavior. The amount of Li consumed forming SEI film is roughly proportional to the surface of all the carbon.[49] In this regard, graphite with spherical structures should produce less SEI film during electrochemical cycling because a spherical structure minimizes the specific surface area. In addition, it has been reported in literature[50-53] that modification of the SEI film may improve the safety of Li-ion cells. For example, a Ni-composite coating consisting of nanoparticles distributed over the surface of the graphite particle[50] effectively blocks some edge surfaces exposed to the electrolyte, thus minimizing solvated lithium intercalation at these edge sites. Similarly, coating the edge surface of the natural graphite by copper has shown to reduce exfoliation.[51] In this study, one spherical natural graphite (GDR) coated with a thin layer of 6 wt % carbon (GDR) was selected for this study. As shown in Fig. 7, Mag-10 has a flake structure and GDR has a spherical structure. The electrochemical cycling performance of the carbon-coated GDR in the first five cycles at 68.6 μA cm^{-2} is shown in Fig. 8. The differential capacity of this sample in the fifth cycle is also shown in the inset plot. The plateau observed in the Mag-10 sample near 0.65 V (Fig. 1) does not appear in the carbon-coated sample, which suggests the SEI formation is suppressed in the CCG sample. SEI formation takes place on both the basal plane and edge plane of the graphite. GDR has the spherical structure which minimizes the specific surface area. Furthermore, carbon coating also decreases the exposure of these planes to the electrolyte, thus decreasing SEI formation. The irreversible capacity for the CCG is only 24 mAh g^{-1} ($\sim$0.065 Li per C_6). The reversible capacity is 338 mAh g^{-1} for Mag-10 and is 340 mAh g^{-1} for carbon-coated GDR. This suggests that CCG is an excellent candidate for Li-ion anode materials with a very high reversible capacity and a very low irreversible capacity.

Figure 9a presents the DSC traces of both anode samples with the composition of $Li_{0.91}C_6$. Figure 9b presents the exothermic heat generations *vs.* temperature for both samples. The CCG shows a smaller normalized heat rate in most temperature ranges, and produces less overall heat generation, suggesting that CCG has better thermal properties than Mag-10. The normalized heat rates and corresponding heat generation due to SEI decomposition are enlarged and shown as inset plots in Fig. 9a and b. It can be seen from these figures that the onset temperatures of the SEI decomposition of both samples are very close, *i.e.*, 83°C for Mag-10 and 84°C for CCG. The CCG sample produces a much smaller normalized heat rate

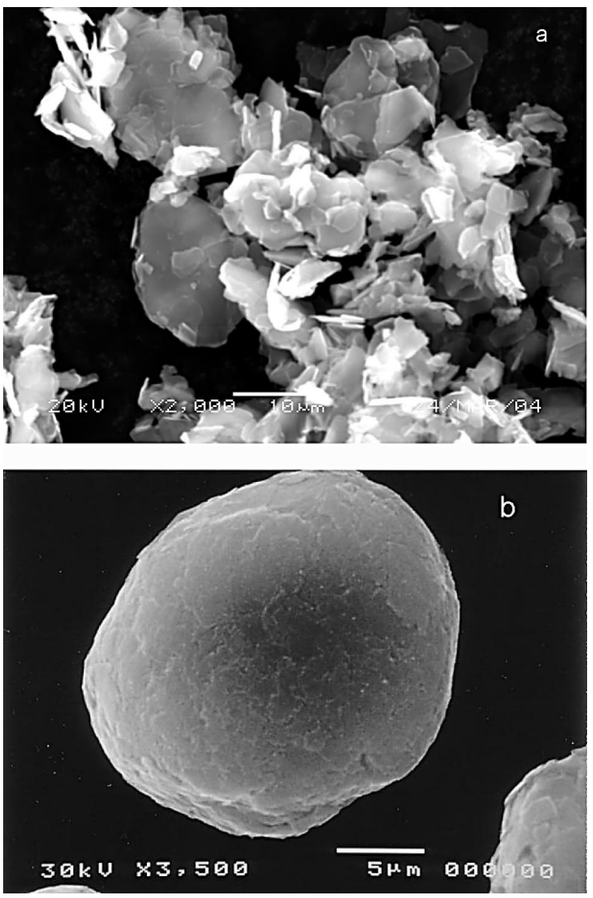

Figure 7. SEM image of sample Mag-10 and carbon coated GDR.

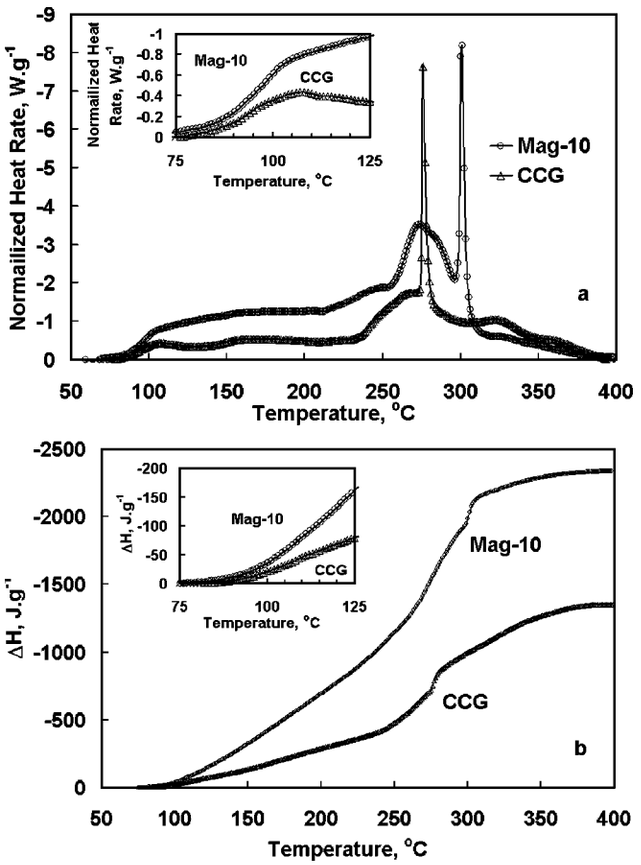

Figure 9. (a) DSC scan of samples Mag-10 and CCG with 0.91 intercalated lithium at a scan rate of 10°C min^{-1}. (b) Overall heat generation of samples Mag-10 and CCG with 0.91 intercalated lithium as a function of temperature.

during SEI breakdown. The enthalpy of the SEI decomposition for CCG is calculated to be $-76\ J\ g^{-1}$, which is far smaller than that of Mag-10 ($-133\ J\ g^{-1}$). The ratio of the enthalpy of the SEI decomposition between the two samples is 1.75, which is exactly equal to the ratio of the irreversible capacity between the two samples. The same ratio of the irreversible capacity and enthalpy of the SEI breakdown indicates that the first peak in the DSC curves is due to the SEI decomposition. The broad peak after the SEI decomposition due to the reaction of the intercalated lithium and the electrolyte is also smaller in the DSC trace of CCG than that of Mag-10 (Fig. 9). The average heat rate of the broad peak for the Mag-10 sample is $-1.25\ W\ g^{-1}$ compared with $-0.5\ W\ g^{-1}$ for the CCG sample. The reason for this difference is that compared to the Mag-10 sample, the CCG sample provides less surface area exposed to the electrolyte to form the secondary SEI film, leading to a smaller heat rate. MacNeil *et al.*[16] showed that the self heat rate in ARC were strongly dependent on the electrochemically accessible surface area of the graphitized samples, increasing by about two orders of magnitude (~0.1 to ~10°C min^{-1}) from the low to the high surface area (0.4 to 9.2 $m^2\ g^{-1}$) of the sample. The overall enthalpy value for the CCG sample from 50 to 270°C is around $-700\ J\ g^{-1}$. As we described earlier, $-76\ J\ g^{-1}$ is produced by SEI breakdown. Thus about $-624\ J\ g^{-1}$ is produced by the formation of the secondary SEI film on the CCG sample. As shown in Fig. 4, about $-1800\ J\ g^{-1}$ heat is produced by SEI breakdown and secondary film formation. Also, 0.37 Li is consumed to form the secondary film and about $-1667\ J\ g^{-1}$ heat is produced in this reaction. Therefore, about 0.14 Li is consumed in the CCG sample to form the secondary SEI film before the graphite structure collapse. The sharp peak due to the structural collapse of Li_xC_6 is also observed for CCG at 276°C; this peak is not detected until 301°C for the Mag-10 sample. The CCG sample consumes fewer intercalated lithium ions, about 0.14, in the formation of the secondary SEI film compared to the 0.37 Li consumed in the Mag-10 sample. Therefore, the CCG sample contains more intercalated lithium ions (0.77) after the reaction to form new stable SEI film which results in a lower onset temperature for the structural collapse reaction. The overall enthalpy

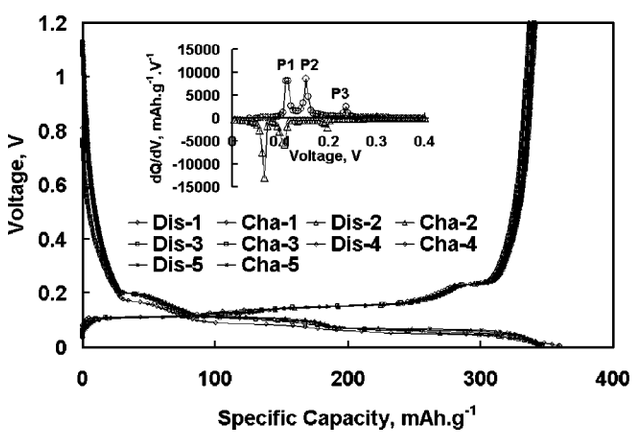

Figure 8. Electrochemical performance of the carbon coated graphite (CCG)/Li half-cell cycled at a current density of 137.2 µA cm^{-2}. Inset plot presents the differential capacity *vs.* voltage for the CCG/Li half-cell.

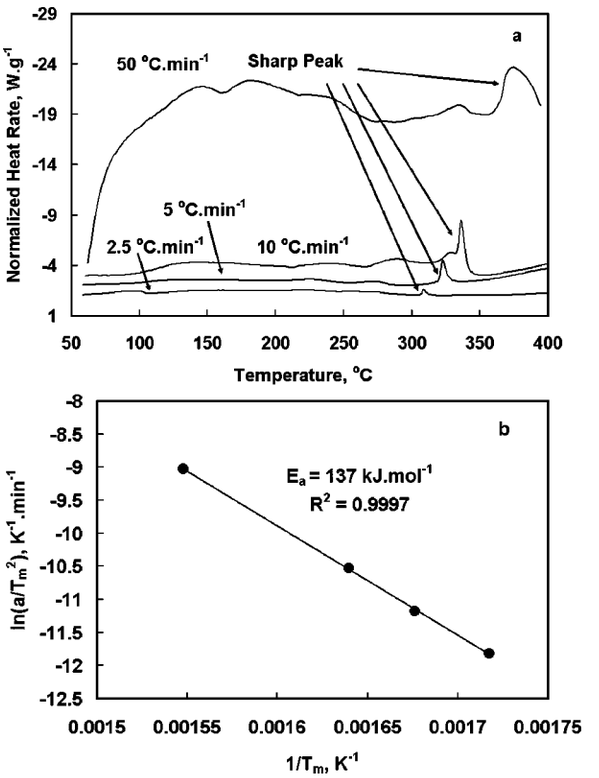

Figure 10. (a) DSC traces of $Li_{0.71}C_6$ at different scan rates. (b) Arrhenius plot of the $Li_{0.71}C_6$ sample.

value for the CCG sample in the range of 50-400°C is only $-1351\ J\ g^{-1}$, which is far less than that of Mag-10 sample ($-2339\ J\ g^{-1}$), Overall, the CCG sample shows much better thermal behavior by producing less heat in the SEI breakdown and reformation. Only 58% of overall heat generation is produced by the CCG sample in the thermal runaway process compared to Mag-10.

The activation energies associated with the structured collapse reaction for $Li_{0.71}C_6$ (Mag-10), $Li_{0.91}C_6$ (Mag-10), and $Li_{0.91}C_6$ (CCG) are determined by performing experiments at different heating rates. The activation energy of SEI decomposition and the formation of the secondary SEI film could not be determined because the peak temperature of these reactions could not be determined accurately due to the severe peak overlap. Figure 10a shows the DSC traces of the $Li_{0.71}C_6$ (Mag-10) anode in the presence of the electrolyte at different scan rates. The increase in the scan rate moves the sharp peak to a higher temperature: 309, 323, 337, and 373°C for heat rates of 2.5, 5, 10, and 50°C min^{-1}, respectively. Also, the increase in the scan rate increases the height of the sharp peak. Figure 10b shows the Arrhenius plots of the $Li_{0.71}C_6$ Mag-10 anode. The DSC traces of the other two samples [$Li_{0.91}C_6$ (Mag-10) and $Li_{0.91}C_6$ (CCG)] at different scan rates show similar behaviors and are not presented here. The activation energies for $Li_{0.71}C_6$ (Mag-10), $Li_{0.91}C_6$ (Mag-10), and $Li_{0.91}C_6$ (CCG) are 137, 108, and 82 kJ mol^{-1}, respectively. When the Li_xC_6 sample collapses, $Li_{0.71}C_6$ contains the least Li and $Li_{0.91}C_6$ (CCG) contains the most Li as shown in Table I. Therefore, the $Li_{0.91}C_6$ (CCG) sample shows the lowest activation energy for the structural collapse reaction and collapses at the lowest temperature.

A possible reaction mechanism for the thermal runaway and structural collapse of the graphite anode can be explained as following. First, the metastable compounds in SEI film break down when the temperature reaches about 80°C. Part of the salt $LiPF_6$ also decomposes at about 70°C to produce LiF and the Lewis acid PF_5.

Table I. Compositions and thermal parameters during structural collapse reaction.

Original sample composition	$Li_{0.71}C_6$ (Mag-10)	$Li_{0.91}C_6$ (Mag-10)	$Li_{0.91}C_6$ (GDR)
Li consumed in the formation of the secondary SEI film	0.37	0.37	0.14
Sample composition when structure collapses	$Li_{0.34}C_6$	$Li_{0.54}C_6$	$Li_{0.77}C_6$
Peak T (°C)	336	300	276
Activation energy (kJ mol^{-1})	137	108	82

The pressure in the DSC sample pans increases due to the expansion of the product gases such as ethylene at high temperatures. Due to the SEI film breakdown, EC and $LiPF_6$ can penetrate the SEI film and reach the edge planes of the lithiated graphite. The intercalated Li is very active at high temperatures and these high temperatures facilitate the movement of Li from the center of the graphite particles to the surface of the edge planes. PF_5 accelerates the Li movement by removing electrons from graphite. A secondary SEI film is formed when the electrolyte reaches the edge plane of the graphite and reacts with the lithium diffusing from the inner structure. This reaction does not stop until either the intercalated Li is consumed completely or products such as Li_2CO_3 and LiF completely block the surface of edge planes. As described earlier, the formation of the secondary SEI film consumes about 0.37 Li. In the formation of the secondary SEI film, some graphite particles break into several smaller pieces while maintaining the bulk structure. The remaining intercalated Li stays in the graphite structure because all the edge planes are now blocked. However, this new Li_xC_6 structure is very active at high temperature and will collapse and release the Li when more than 0.3 Li remains in the C_6. The more intercalated lithium remaining ($\geqslant$0.34 Li) renders the structure more unstable and results in lower activation energy for this structural collapse reaction which occurs at a lower temperature (as shown in Table I). The released Li as a result of the structural collapse reacts with the PVDF binder to form LiF and hydrogen.

Conclusions

Thermal behavior of the natural graphite anode (Mag-10) at different states of charge are studied using DSC. The Li_0C_6 sample shows one exothermic peak, which is attributed to the SEI decomposition. Anode samples with more intercalated lithium produce broad DSC peaks following SEI film decomposition, and are attributed to the formation of a secondary SEI film. The graphite structure collapses at high temperatures for samples containing more than 0.71 lithium per C_6. A sharp peak observed in the DSC scan has been attributed to the structural collapse of graphite. It is also concluded that PVDF binder is not responsible for this sharp peak. However, Li released from graphite particle reacts with the PVDF to produce more heat. Carbon-coated spherical graphite particles improve the thermal stability of the graphite anode. Carbon coating modifies the SEI film and blocks the edge planes in the graphite. Blocking of the edge planes reduces the formation of a secondary SEI film and hence reduces the heat produced due to the decomposition of the secondary SEI film.

Acknowledgment

This work was supported by the Chemical Technology Division of the Argonne National Laboratory. The authors are grateful to Gary Henriksen, and Dr. Jun Liu of the Chemical Technology Division, Argonne National Laboratory for their encouragement and support.

Illinois Institute of Technology assisted in meeting the publication costs of this article.

References

1. S. Tobishima, Y. Sakurai, and J. Yamaki, *J. Power Sources*, **68**, 445 (1997).
2. K. Kitoh and H. Nemoto, *J. Power Sources*, **81-82**, 887 (1999).
3. S. Passerini, F. Coustier, and B. B. Owens, *J. Power Sources*, **90**, 144 (2000).
4. S. Tobishima, K. Takei, U. Sakurai, and J. Yamaki, *J. Power Sources*, **90**, 188 (2000).
5. C. W. Lee, R. Venkatachalapathy, and J. Prakash, *Electrochem. Solid-State Lett.*, **3**, 63 (2000).
6. T. Ohsuku and Y. Makimura, *Chem. Lett.*, **30**, 642 (2001).
7. Z. Lu, D. D. MacNeil, and J. R. Dahn, *Electrochem. Solid-State Lett.*, **4**, A191 (2001).
8. Z. Lu, D. D. MacNeil, and J. R. Dahn, *Electrochem. Solid-State Lett.*, **4**, A200 (2001).
9. K. Xu, S. Zhang, T. Richard Jow, W. Xu, and C. A. Angell, *Electrochem. Solid-State Lett.*, **5**, A26 (2002).
10. M. Ihara, B. T. Hang, K. Sato, M. Egashira, S. Okada, and J.-I. Yamaki, *J. Electrochem. Soc.*, **150**, A1476 (2003).
11. H. Yang, Ph.D. Thesis, Illinois Institute of Technology, Chicago, IL (2004).
12. H. Maleki, G. Deng, A. Anani, and J. Howard, *J. Electrochem. Soc.*, **146**, 3224 (1999).
13. U. von Sacken, E. Nodwell, A. Sundher, and J. R. Dahn, *J. Power Sources*, **54**, 240 (1995).
14. U. von Sacken, E. Nodwell, A. Sundher, and J. R. Dahn, *Solid State Ionics*, **69**, 284 (1994).
15. Z. Zhang, D. Fouchard, and J. R. Rea, *J. Power Sources*, **70**, 16 (1998).
16. D. D. MacNeil, D. Larcher, and J. R. Dahn, *J. Electrochem. Soc.*, **146**, 3596 (1999).
17. M. N. Richard and J. R. Dahn, *J. Electrochem. Soc.*, **146**, 2068 (1999).
18. K. Edstrom and M. Herranen, *J. Electrochem. Soc.*, **147**, 3628 (2000).
19. R. Venkatachalapathy, C. W. Lee, W. Lu, and J. Prakash, *Electrochem. Commun.*, **2**, 104 (2000).
20. A. M. Andersson, K. Edstrom, N. Rao, and A. Wendsjo, *J. Power Sources*, **81-82**, 286 (1999).
21. H. Maleki, G. Deng, I. Kerzhner-Haller, A. Anani, and J. N. Howard, *J. Electrochem. Soc.*, **147**, 4470 (2000).
22. G. Botte, R. White, and A. Zhang, *J. Power Sources*, **97-98**, 570 (2001).
23. D. D. MacNeil and J. R. Dahn, *J. Electrochem. Soc.*, **149**, A912 (2002).
24. J. Yamaki, H. Takatsuji, T. Kawamura, and M. Egashira, *Solid State Ionics*, **148**, 241 (2002).
25. J. S. Gnanaraj, E. Zinigrad, L. Asraf, H. E. Gottlieb, M. Sprecher, M. Schmidt, W. Geissler, and D. Aurbach, *J. Electrochem. Soc.*, **150**, A1533 (2003).
26. H. H. Lee, C. C. Wan, and Y. Y. Wang, *J. Electrochem. Soc.*, **151**, A542 (2004).
27. T. Zheng, A. S. Gozdz, and G. G. Amatucci, *J. Electrochem. Soc.*, **146**, 4014 (1999).
28. K. Kanamura, H. Tamura, S. Shiraishi, and Z. Takechedra, *J. Electroanal. Chem.*, **394**, 49 (1995).
29. D. Aurbach, Y. Ein-Eli, B. Markovsky, A. Zaban, S. Luski, Y. Carmeli, and H. Yamin, *J. Electrochem. Soc.*, **142**, 2882 (1995).
30. E. Peled, *J. Electrochem. Soc.*, **126**, 2047 (1979).
31. A. N. Dey and B. P. Sullivan, *J. Electrochem. Soc.*, **117**, 222 (1970).
32. J.-L. McNaughton and C.-T. Mortiner, *Thermochemistry and Thermodynamics*, *Physical Chemistry*, International Review of Science, Boston, MA, Series Two, p. 10 (1975).
33. T. Ozawa, *J. Therm. Anal.*, **2**, 301 (1970).
34. J. R. Dahn, *Phys. Rev. B*, **44**, 9170 (1991).
35. P. A. Derosa and P. B. Balbuena, *J. Electrochem. Soc.*, **146**, 3630 (1999).
36. E. Peled, D. Golodnitsky, and G. Ardel, *J. Electrochem. Soc.*, **144**, L208 (1997).
37. X. Zhang, P. N. Ross, J. R. Kostecki, F. Kong, S. Sloop, J. B. Kerr, K. Striebel, E. J. Cairns, and J. McLarono, *J. Electrochem. Soc.*, **148**, A463 (2001).
38. S. E. Sloop, J. K. Pugh, S. Wang, J. B. Kerr, and K. Kinoshita, *Electrochem. Solid-State Lett.*, **4**, A42 (2001).
39. T. Kawamura, A. Kimura, M. Egashira, S. Okada, and J. I. Yamaki, *J. Power Sources*, **104**, 260 (2002).
40. K. Kanamura, H. Tamura, and Z. Takehara, *J. Electroanal. Chem.*, **333**, 127 (1999).
41. A. M. Andersson and K. Edstrom, *J. Electrochem. Soc.*, **148**, A1100 (2001).
42. D. Bar Tow, E. Peled, and L. Burstein, *J. Electrochem. Soc.*, **146**, 824 (1999).
43. K. Edstrom, T. Gustafsson, and J. O. Thomas, in *Lithium Batteries*, G. S. Surampudi and R. Marsh, Editors, PV 98-16, p. 117, The Electrochemical Society Proceedings Series, Pennington, NJ (1999).
44. D. Aurbach, A. Zaban, Y. Ein-Eli, I. Weissman, O. Chusid, B. Markovsky, M. Levi, E. Levi, A. Schechter, and E. Granot, *J. Power Sources*, **68**, 91 (1997).
45. A. Du Pasquier, F. Disma, T. Bowmer, A. S. Gozdaz, G. Amatucci, and J.-M. Tarascon, *J. Electrochem. Soc.*, **145**, 472 (1998).
46. Z. Jiang, M. Alamgir, and K. M. Abraham, *J. Electrochem. Soc.*, **142**, 333 (1995).
47. G.-C. Chung, H.-J. Kim, S.-I. Yu, S.-H. Jun, J.-W. Choi, and M.-H. Kim, *J. Electrochem. Soc.*, **147**, 4391 (2000).
48. G. M. Gray, *Solid Polymer Electrolytes-Fundamental and Technological Applications*, VCH, New York (1991).
49. R. Fong, U. von Sacken, and J. R. Fahn, *J. Electrochem. Soc.*, **137**, 2009 (1990).
50. P. Yu, J. A. Ritter, R. E. White, and B. N. Popov, *J. Electrochem. Soc.*, **147**, 1280 (2000).
51. W. Lu, V. S. Donepudi, J. Prakash, J. Liu, and K. Amine, *Electrochim. Acta*, **47**, 1601 (2002).
52. M. Yoshio, H. Wang, K. Fukuda, Y. Hara, and Y. Adachi, *J. Electrochem. Soc.*, **147**, 1245 (2000).
53. H. Wang and M. Yoshio, *J. Power Sources*, **93**, 123 (2001).